Limits to the symmetry of a Mach-Zehnder-type atom interferometer

P. Gillot, B. Cheng, S. Merlet, and F. Pereira Dos Santos*

LNE-SYRTE, Observatoire de Paris, PSL Research University, CNRS, Sorbonne Universités, UPMC Univ. Paris 06, 61 Avenue de l'Observatoire, 75014 Paris, France

(Received 3 April 2015; published 12 January 2016)

Owing to the use of a symmetrization π pulse at the middle of their laser sequences, Mach-Zehnder-type atom interferometers are insensitive to clocks shifts and Doppler shifts, if constant, but to changes in these quantities, which makes them accurate and sensitive inertial-force sensors. However, variations of the Raman laser coupling between laser pulses restore a parasitic sensitivity to the Doppler shift. This effect, which sets a limit to the symmetry of the interferometer, is quantitatively evaluated here as a function of the experimental parameters, in the case of an atom gravimeter experiment, and compared to expectations. We show in particular that velocity-distribution asymmetries lead to parasitic phase shifts that can compromise the accuracy and long-term stability of the gravity measurement in the low $10^{-9}g$ range.

DOI: 10.1103/PhysRevA.93.013609

I. INTRODUCTION

Quantum technologies, which are based on the coherent manipulation and control of quantum states, exploit quantum superposition of states that allow for improved performances in communication [1] and computing protocols [2], in atom-interferometry-based inertial sensing [3,4], timekeeping [5], or magnetometry [6]. The coherence of such quantum states needs to be preserved from decoherence or dephasing arising from inhomogeneities in coupling or resonance conditions. Various techniques have been developed for that purpose based on adiabatic passage techniques [7,8], pulse shaping, or spin echo techniques [9], with NMR being a domain in which this engineering reaches its highest degree of sophistication, with a large variety of complex pulse sequences having been developed for a precise tailoring of the state evolution [10].

In the context of atom interferometry [11], which is our interest here, analogous techniques have been used to separate the effect of inertial forces, which act on the external degrees of freedom, from a certain number of phase shifts related to the internal structure of the atoms. In particular, in Raman interferometers where a sequence of three Raman pulses allow splitting, redirecting, and recombining the partial wave packets [12,13], the middle π pulse not only allows the wave packets to be redirected towards each other, but also exchanges internal states. As a consequence, the phase shift accumulated during the first half of the interferometer, if related to clock shifts (i.e., to shifts of the electronic energy levels), is compensated by the phase shift accumulated during its second half. In principle, this symmetric interferometer geometry makes the interferometer insensitive to the detuning of the Raman beams from resonance, in contrast with a clock based on the traditional two-pulse Ramsey sequence [14].

In practice, as already claimed in Ref. [13], small residual phase offsets can appear when the Raman frequency is not perfectly centered with respect to the atomic Doppler distribution. In particular, the authors of Ref. [13] observed that their measured value of g shifted by 1 μGal/kHz when they varied the frequency of their coupling laser beams (1 $\mu\text{Gal} = 10^{-8}$ m/s^2), but they did not provide a detailed analysis of this effect at that time. This was, to our knowledge, the first discussion of this topic, and we are not aware of any later detailed study of this effect.

The aim of this paper is thus to provide a quantitative analysis of these residual offsets and of their dependence on experimental parameters. We show in particular that, in the general case where the couplings are different for the different pulses, the symmetry of the interferometer is broken, so that it exhibits a residual sensitivity to Doppler shifts. As a case study, we investigate the impact of this asymmetry on the gravity measurements performed with a Mach-Zehnder interferometer in a gravimeter configuration.

We start by investigating this effect theoretically in the first section of the paper. We then describe our gravimeter experiment, focusing on the features most relevant for this study and detailing our measurement process. In particular, the expansion of the atoms inside the Raman beams during the interferometer induces differences in the Raman coupling at each pulse. We then investigate the sensitivity of the gravity measurement to the interferometer asymmetry by modifying the velocity distribution of the detected atoms. Finally, we introduce controlled asymmetries by deliberately changing the intensity in the last Raman pulse and demonstrate the possibility to compensate the effect of the asymmetry arising from the expansion of the cloud.

II. ASYMMETRY OF ATOMIC INTERFEROMETER

The Mach-Zehnder interferometer is implemented by using a three pulses sequence ($\pi/2$-π-$\pi/2$) of counterpropagating Raman transitions [12]. These pulses respectively separate, redirect, and finally recombine the two partial wave packets. The phase $\Delta\Phi$ at the output of the interferometer is given by a linear combination of the phase difference of the Raman lasers at each of the three pulses $\Delta\Phi = \phi_1 - 2\phi_2 + \phi_3$ [11]. Assuming perfect and infinitesimally short Raman pulses, and neglecting any contributions other than the one related to the spatial dependence of the Raman laser phase difference, this phase ϕ_i is linked to the position of the atom wave packet with

*franck.pereira@obspm.fr

respect to the phase front of the Raman laser $\phi_i = \vec{k}_{\rm eff} \cdot \vec{r}_i$. The phase of the interferometer thus provides a three-point measurement of the trajectories of the atoms. Here, $\vec{k}_{\rm eff} = \vec{k}_1 - \vec{k}_2$ is the effective wave vector of the Raman process, $\vec{k}_1$ and $\vec{k}_2$ are the wave vectors of the Raman lasers, and $\vec{r}_i$ is the position of the atoms at the ith pulse. If the time separation between consecutive pulses is equal, this linear combination allows us to extract the curvature of the atoms' trajectories (and thus their acceleration) independently of the initial velocity. More generally, a linear increase in the difference between atomic and laser phases, such as due to a detuning from the Raman resonance condition arising either from frequency shifts of the internal energy levels or a Doppler shift of the atoms, makes no contribution to the interferometer phase. When using counterpropagating Raman lasers, the geometry of the Mach-Zehnder interferometer and, more specifically, its symmetry makes this interferometer an inertial sensor and not a clock.

Nevertheless, this cancellation relies on the perfect symmetry of the two $\pi/2$ pulses. We show here that, for finite pulse durations, nonzero Raman detunings, and unequal pulse intensities, the interferometer becomes sensitive to noninertial effects. For that purpose, we calculate the evolution throughout the whole interferometer of the atomic wave function, in the basis of the two states that are coupled by the Raman lasers, for Raman pulses of finite durations, and following a treatment similar to Refs. [15–17]. The detuning δ from resonance is given by

$$\delta = \omega_2 - \omega_1 - (\omega_0 + \omega_{\rm D} + \omega_{\rm R} + \omega_{\rm LS}), \tag{1}$$

where ω_1 and ω_2 are the frequencies of the two Raman lasers, ω_0 is the frequency of the hyperfine transition, $\omega_{\rm D} = \vec{k}_{\rm eff} \cdot \vec{v}$ is the Doppler shift, $\omega_{\rm R}$ is the recoil frequency, and $\omega_{\rm LS}$ is the (possibly uncompensated) differential light shift from the Raman lasers. The two-photon Rabi frequencies are taken to be potentially different for each pulse, given by Ω_i for the ith pulse. Although the interferometer pulses can thus differ from perfect $\pi/2$ and π pulses, we will continue throughout the rest of the paper to refer to them as such. After some algebra, we find an additional contribution to the phase of the interferometer given by

$$\Delta\Phi = \arg\left(\cos\left(\frac{1}{2}\tau\sqrt{\delta^2+\Omega_1^2}\right) - \frac{i\delta\sin\left(\frac{1}{2}\tau\sqrt{\delta^2+\Omega_1^2}\right)}{\sqrt{\delta^2+\Omega_1^2}}\right) + \arg\left(\cos\left(\frac{1}{2}\tau\sqrt{\delta^2+\Omega_3^2}\right) + \frac{i\delta\sin\left(\frac{1}{2}\tau\sqrt{\delta^2+\Omega_3^2}\right)}{\sqrt{\delta^2+\Omega_3^2}}\right), \tag{2}$$

where τ is the duration of the first and last pulse. This shows that the phase of the interferometer is independent of Ω_2, but shows a residual sensitivity to a fixed detuning if Ω_1 is different from Ω_3.

Figure 1 displays as a dotted line this phase shift for the following parameters: $\Omega_1 = 2\pi \times 25$ kHz, $\Omega_3 = 1.1\Omega_1$, and $\tau = 10$ μs. Significant phase shifts, of several tens of mrad, are calculated for detunings of the order of the Rabi frequency. In our experiment, the width of the velocity distribution results in a distribution of detuning due to the Doppler shift, so that the phase of the interferometer results from an averaging of the phase shift calculated in Eq. (2) over this distribution.

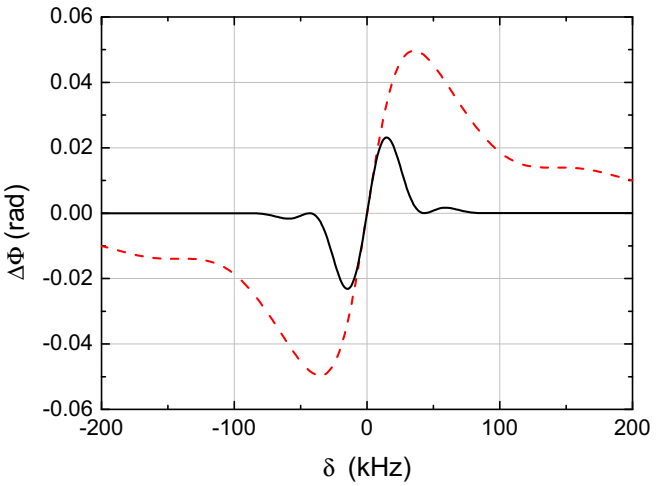

FIG. 1. Interferometer phase shift as a function of the detuning with respect to the Raman resonance condition, for a difference of 10% in couplings Ω between the first and last Raman pulse. The dotted line is the unweighted contribution, calculated by using Eq. (2). The thick line is weighted by the contrast.

We now show how to perform this averaging by considering how each velocity class contributes to the interferometer phase. Let us consider the fraction of atoms of velocity v within dv, given by $Nf(v)dv$. N is the total number of atoms and $f(v)$ is their velocity distribution. These atoms, which enter the interferometer in the ground state $|g\rangle$ ($|5S_{1/2}, F = 1\rangle$ for ^{87}Rb), exit the interferometer in the excited state $|e\rangle$ ($|5S_{1/2}, F = 2\rangle$ for ^{87}Rb) with a certain transition probability $P(v)$ that depends on v. This transition probability is calculated by using the method described above and is written as $P(v) = A(v) + \frac{1}{2}C(v)\cos[\Phi_0 + \Delta\Phi(v)]$, where Φ_0 is a phase that is independent of the velocity v (being, for instance, the inertial phase) and $\Delta\Phi(v)$ is the phase shift calculated above. $A(v)$ is an offset and $C(v)$ is interpreted as the contrast with which this velocity class realizes the interferometer. The total number of atoms exiting in the state $|e\rangle$ is thus given by $N_e = N\int f(v)P(v)dv$, and the transition probability of the interferometer, defined as $P = N_e/N$, is given by $P = \int f(v)P(v)dv$. Assuming that $\Delta\Phi(v)$ remains small with respect to 1 rad for significant values of $f(v)$, this simplifies to $P \simeq A + \frac{1}{2}C\cos(\Phi_0 + \overline{\Delta\Phi})$, with $C = \int f(v)C(v)dv$ and $\overline{\Delta\Phi} = \frac{1}{C}\int f(v)C(v)\Delta\Phi(v)dv$.

This shows that the contribution to the interferometer phase shift $\overline{\Delta\Phi(v)}$ of each velocity class is weighted not only by the velocity distribution but also by its (normalized) contribution to the global contrast. We give below the analytic expression of the contrast $C(\delta)$ for a given detuning δ (one simply has to

replace δ by $k_{\text{eff}}v$ for a Doppler shift):

$$C(\delta) = \frac{4\Omega_1\Omega_2^2\Omega_3 \sin^2\left(\tau\sqrt{\delta^2+\Omega_2^2}\right)\sin\left(\frac{1}{2}\tau\sqrt{\delta^2+\Omega_1^2}\right)\sin\left(\frac{1}{2}\tau\sqrt{\delta^2+\Omega_3^2}\right)}{\left(\delta^2+\Omega_1^2\right)\left(\delta^2+\Omega_2^2\right)\left(\delta^2+\Omega_3^2\right)}$$
$$\times\left[\delta^2\sin\left(\frac{1}{2}\tau\sqrt{\delta^2+\Omega_1^2}\right)\sin\left(\frac{1}{2}\tau\sqrt{\delta^2+\Omega_3^2}\right)+\sqrt{\delta^2+\Omega_1^2}\sqrt{\delta^2+\Omega_3^2}\cos\left(\frac{1}{2}\tau\sqrt{\delta^2+\Omega_1^2}\right)\cos\left(\frac{1}{2}\tau\sqrt{\delta^2+\Omega_3^2}\right)\right]. \quad (3)$$

The phase shift $\Delta\Phi(\delta)$ multiplied by the contrast $C(\delta)$ is finally displayed as a thick line on Fig. 1. The figure clearly shows that the weighting by the contrast $C(\delta)$ reduces the contribution of large detunings classes. The odd character of the weighted phase shift makes the overall phase $\overline{\Delta\Phi}$ equal zero if the velocity distribution is symmetric and the Raman resonance condition is tuned to the center of the distribution. By contrast, any asymmetry of the distribution or off-centering of the Raman resonance will result in a parasitic phase shift leading to systematic errors in the inertial measurement.

III. EXPERIMENTAL SETUP

A. Interferometer setup

In our setup, ^{87}Rb atoms from a two-dimensional magneto-optical trap (2D-MOT) load a three-dimensional MOT (3D-MOT) for about 80 ms [18]. A subsequent molasses phase cools the atoms down to a temperature of about 2 μK. The molasses beams are then simultaneously switched off within 100 μs with a fast mechanical shutter. The atomic cloud, whose $1/e^2$ radius is 0.5 mm, is thus simply allowed to freely fall over a distance of about 20 cm before being detected at the bottom of the vacuum chamber. Although their initial velocity is in principle null, fluctuations in the imbalance between the molasses beams of a few percent, as well as in their polarizations, lead to residual velocity fluctuations of up to 100 μm/s.

The atoms are vertically velocity selected [15] in the $|F=1,m_F=0\rangle$ state thanks to a combination of microwave, pusher, and Raman pulses. In more detail, a first microwave pulse transfers about 1/5 of the atoms, initially in the $|F=2\rangle$ state, into the $|F=1,m_F=0\rangle$ state. A brief pulse of a pusher beam, tuned on the $|F=2\rangle \rightarrow |F'=3\rangle$ transition, removes atoms left in $|F=2\rangle$. A second microwave pulse transfers the remaining atoms in the $|F=2,m_F=0\rangle$ state, before a Raman selection pulse is applied, which transfers the central part of the velocity distribution into $|F=1,m_F=0\rangle$. Finally, a second pusher pulse removes the atoms left in $|F=2\rangle$, which have not been selected. The maximum two-photon Rabi frequency of the Raman pulse is of the order of $2\pi \times 25$ kHz, comparable to the Doppler width of the initial velocity distribution. The single-frequency detuning of the Raman lasers is of order of -1 GHz, and the $1/e^2$ radius of the Raman beams is 12 mm. After selecting the atoms, we drive a Mach-Zehnder interferometer, using a $\pi/2$-π-$\pi/2$ Raman pulse sequence, to respectively separate, redirect, and finally recombine the two partial wave packets [12]. The first pulse of the interferometer occurs about 16 ms after the release from the molasses. The Rabi frequency for the interferometer is identical to the Rabi frequency used in the selection. This ensures that the difference in the resonance condition between the selection and the first Raman pulse is linked to the 4-ms time separation between these two pulses only and is independent of the Raman differential light shift if any. This time separation induces a Doppler-shift change of 100.5 kHz, which is precisely accounted for in the experiments presented below, except when otherwise specified. On the contrary, changing the Rabi frequency in between the selection and the interferometer would induce a change in the same proportion of the differential light shift if the latter is not canceled (this cancellation can be realized by a proper adjustment of the intensity ratio between the Raman lasers). This change in light shift would also need to be accounted for in order for the Raman pulse to be tuned on resonance for the interferometer.

We exploit the state labeling [11] to measure the populations in the two output states, thanks to a detection performed on the internal state. From the populations N_1 and N_2 in the two hyperfine states, we derive the transition probability $P = N_1/(N_1+N_2)$. This transition probability P is given by $P = \frac{1}{2}[1 + C\cos(\Delta\Phi)]$, where C is the interferometer contrast and $\Delta\Phi$ is the phase difference between the two different arms. In our geometry of vertically aligned Raman lasers, this phase shift is given by $\Delta\Phi = k_{\text{eff}}gT^2$ [19], where g is the gravity acceleration, and $T = 80$ ms is the time separation between consecutive pulses. The cycle time in our experiment is 360 ms.

B. Detection setup

As will be shown later, the response of the detection, which weights differently the contribution of the different velocity classes to the interferometer signal, induces residual noninertial phase shifts due to the asymmetry of the interferometer. We thus describe here the main features of the detection system, which allows for simultaneous detection of the two populations. A more detailed description can be found in Ref. [18]. The atoms arrive in the detection zone about 200 ms after their release from the molasses, and 20 ms after the last $\pi/2$ pulse. Their velocity in the detection area is thus 2 m/s. For the detection phase, the two lasers which induce Raman transitions during the selection and interferometer phase are put on resonance with respectively the $|F=1\rangle \rightarrow |F'=2\rangle$ (repumping) and $|F=2\rangle \rightarrow |F'=3\rangle$ (cycling) transitions. A first brief pulse of duration of 90 μs resonant with the $|F=2\rangle \rightarrow |F'=3\rangle$ transition freezes the atoms in the $|F=2\rangle$ state while the $|F=1\rangle$ atoms continue to fall [20,21]. After a separation time of about 10 ms, the two clouds are 2 cm apart. A 10-ms-long pulse containing both slightly red detuned cycling light and on-resonance repumping light then illuminates the two clouds with a high saturation parameter ($s \sim 50$). The emitted fluorescence is collected onto

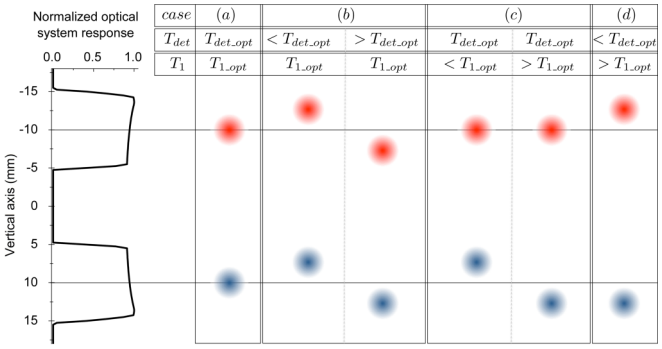

FIG. 2. Positions of the two atomic populations in the detection area for different timing parameters ($T_{\rm det}$ and T_1). The $|F=2\rangle$ ($|F=1\rangle$) state is represented in red (blue). On the left, the normalized optical system response is displayed along the vertical axis z. $z=0$ is taken as the vertical center of the detection system. (a) Optimal case: the two populations are centered on their respective detection zones (-10 mm and $+10$ mm) corresponding to the optimal pair ($T_{\rm det}=T_{\rm det\_opt}$ and $T_1=T_{1\_opt}$). (b) Off-centered case: $T_{\rm det}\neq T_{\rm det\_opt}$ and $T_1=T_{1\_opt}$. (c) Case where one cloud only is well centered in its corresponding detection zone $T_{\rm det}=T_{\rm det\_opt}$ and $T_1\neq T_{1\_opt}$. (d) $T_{\rm det}\neq T_{\rm det\_opt}$ and $T_1\neq T_{1\_opt}$.

two different photodiodes, one for each of the two populations. The timing of both the brief pulse (at $T_{\rm det}$) and the long pulse (at $T_{\rm det}+T_1$) is set so as to optimize the positioning of the two atom clouds in each of the two detection zones.

Figure 2 displays a sketch of the detection system and illustrates the effect of the parameters $T_{\rm det}$ and T_1 in different cases. It displays on the left the theoretical response of the detection system along the vertical axis. Measurements of its actual response are in good agreement with the expectations of the model, with maximum deviations of only 4% [18]. One can notice that the response of each measurement zones is not flat, but varies almost linearly by about 9%, with an opposite slope for each zones. The optical system that collects the fluorescence being the same for the detection of the two zones, the photodiodes are offset with respect to the optical axis of the system, which leads to an inhomogeneous response as a function of the initial position of the atoms in a given zone. Actually, this detection system was designed to guarantee a flat response of the detection efficiency in the transverse plane (and not necessarily in the vertical direction) in order to efficiently average to zero Coriolis-acceleration phase shifts [18]. Given that response, detecting the atoms off center as displayed as case (d) in Fig. 2 maximizes the signal, but, as we will see later, leads to a bias in the measurement.

C. Measurement process

In our experiment, the usual g absolute measurement is performed by alternating measurements in four different configurations [18]. This measurement protocol allows most of the systematic effects to be removed, except Coriolis acceleration and eventual phase shifts due to wavefront distortions. It is composed of two pairs of configurations in which the wave vector $k_{\rm eff}$ is reversed ($k_\uparrow$ and $k_\downarrow$). $k_{\rm eff}=k_\uparrow$ describes the situation where the higher-frequency Raman beam propagates upward, and $k_{\rm eff}=k_\downarrow$ describes where the higher-frequency beam propagates downward. The half difference of a single pair of configuration ($k_\uparrow$ and $k_\downarrow$) provides a $g_{\uparrow\downarrow}$ measurement in which the effects related to perturbations of the internal degrees of freedom of the atoms and to radio-frequency phase shift are suppressed [13]. The second pair is performed with half the Raman power, which allows the two-photon light shift to be suppressed [22]. For most of the measurements performed in this paper, we also alternate four configurations. A first pair of $k_\uparrow$ and $k_\downarrow$ configurations with fixed parameters leads to a reference value of $g^{\rm ref}_{\uparrow\downarrow}$, whereas we modify one or few parameters in the second pair. We thus perform differential gravity measurements $\Delta g=g^{\rm ref}_{\uparrow\downarrow}-g^{\rm mod}_{\uparrow\downarrow}$, where common-mode effects (related, for instance, to real gravity changes, such as tides, or most of the systematic effects, such as Coriolis acceleration) are rejected.

IV. EFFECT OF INITIAL VERTICAL RAMAN SELECTION

We start by modifying the selection parameters to investigate the impact on the gravity measurement of the shape of the velocity distribution of the selected atoms. Figure 3 illustrates how the shape of this velocity distribution can be altered. Although the initial velocity distribution in our experiment is better described by a Lorentzian b, as already discussed in Ref. [23] and given by $f(v)=A/[1+(v-v_0)^2/v_{\rm c}^2]^b$, than a Gaussian, as we will see later, we take here for this illustration the initial velocity distribution to be Gaussian, with a FWHM of 80 kHz, which corresponds to a temperature of 1.8 μK and which is comparable to the FWHM of the velocity distribution in the experiment.

After the selection pulse, performed with a Raman pulse along the vertical direction, of frequency $\nu_{{\rm sel}\uparrow}$ ($\nu_{{\rm sel}\downarrow}$) for a $k_\uparrow$ configuration measurement ($k_\downarrow$), the selected velocity distribution enters the interferometer. In the absence of Raman detuning at the selection, the Raman frequencies $\nu_{{\rm sel}\uparrow}$ and $\nu_{{\rm sel}\downarrow}$ correspond to Raman pulses tuned on resonance with the center of the velocity distribution. But, by modifying the selection frequency by $\delta\nu_{\rm sel}$, we can prepare a velocity distribution with a controllable asymmetry. Depending on whether we offset the selection frequency in the same or in opposite directions for the $k_\uparrow$ and $k_\downarrow$ measurements, we generate two different ways to potentially bias the gravity measurement:

(i) The first case, where we apply opposite offsets to the selection frequencies ($\nu_{{\rm sel}\downarrow}+\delta\nu_{\rm sel}$; $\nu_{{\rm sel}\uparrow}-\delta\nu_{\rm sel}$), mimics an error in the determination of the mean Doppler shift at the selection.

(ii) The second case ($\nu_{{\rm sel}\downarrow}+\delta\nu_{\rm sel}$; $\nu_{{\rm sel}\uparrow}+\delta\nu_{\rm sel}$) mimics the effect of a residual uncompensated one-photon light shift.

Figure 3 displays the calculated selected velocity distribution obtained for various settings of the selection frequency. Figure 3(b) corresponds to selection frequencies well centered on the velocity distribution, which lead to symmetric selected velocity distributions. Figures 3(c) and 3(d) correspond to the two cases discussed above and lead to asymmetric velocity distributions. In particular, one can notice a clear difference Δ in the amplitudes of the secondary lobes on either side of the distribution.

We then measure the impact on the gravity determination in these two cases by performing differential measurements using the four configuration-measurement processes detailed above.

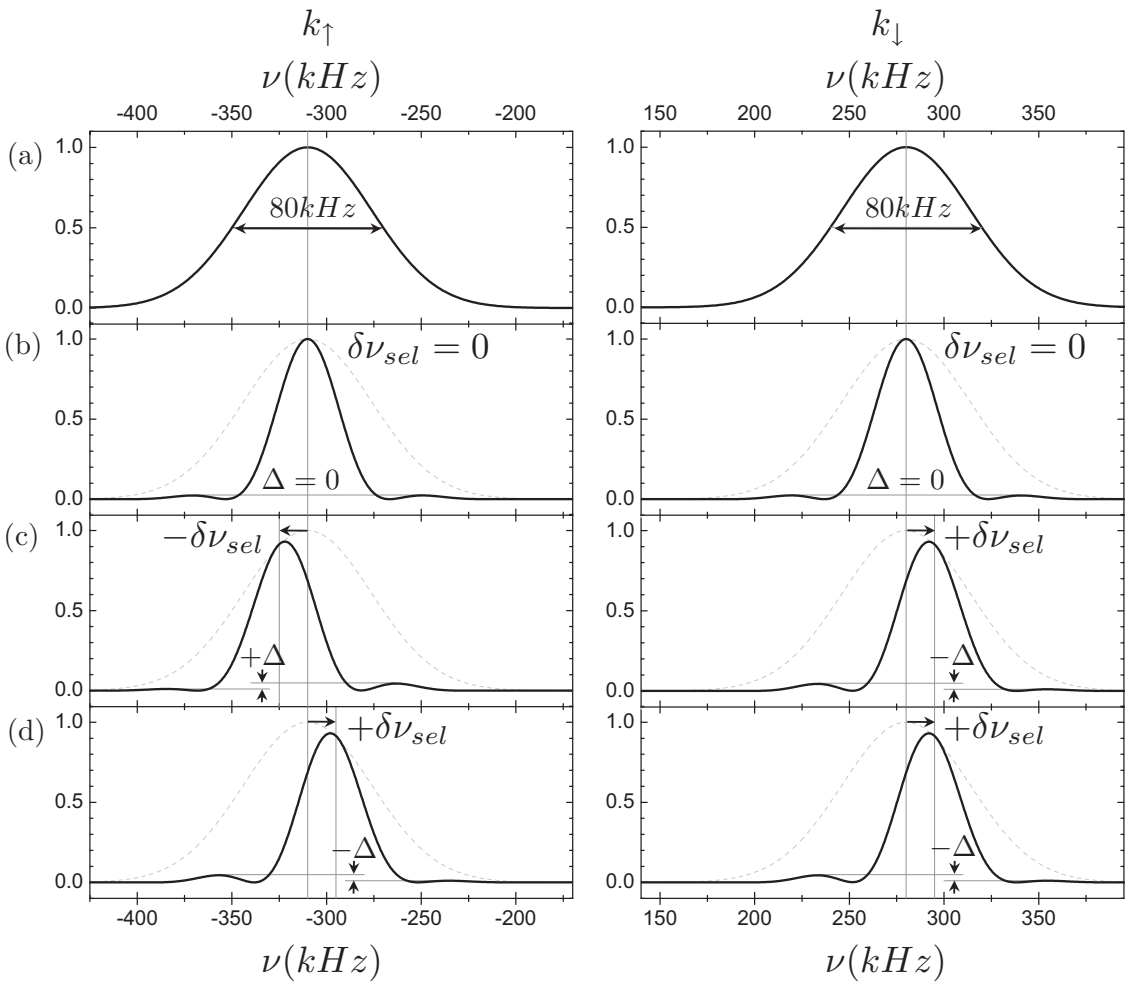

FIG. 3. Predicted velocity distributions (in the frequency domain) (a) before and (b)–(d) after the vertical velocity Raman selection pulse. The spectra on the left correspond to the $k_\uparrow$ configuration, and the ones on the right to the $k_\downarrow$ configuration. The horizontal-axis label ν corresponds to the resonant frequency of each velocity class, offset by the frequency of the hyperfine transition. (a) Initial Gaussian distribution. The centers of the distribution are $\nu_{\mathrm{sel}\uparrow} = -310$ kHz in the $k_\uparrow$ configuration and $\nu_{\mathrm{sel}\downarrow} = 280$ kHz in the $k_\downarrow$ one. (b) Velocity distribution after the selection in the ideal case, for which $\delta\nu_{\mathrm{sel}} = 0$. (c) Case where $\delta\nu_{\mathrm{sel}} \neq 0$ and where the selection frequencies are offset in opposite directions: $\nu_{\mathrm{sel}\uparrow}$ is shifted by $-\delta\nu_{\mathrm{sel}}$ and $\nu_{\mathrm{sel}\downarrow}$ by $+\delta\nu_{\mathrm{sel}}$. This case corresponds to a Doppler effect. (d) Case where $\delta\nu_{\mathrm{sel}} \neq 0$ and where the selection frequencies are offset in the same direction: $\nu_{\mathrm{sel}\uparrow}$ is shifted by $+\delta\nu_{\mathrm{sel}}$ and $\nu_{\mathrm{sel}\downarrow}$ by $+\delta\nu_{\mathrm{sel}}$. This case corresponds to a one-photon light shift. Δ is the difference in amplitude between the two second-order lobes of the selected velocity distribution.

As discussed above, the Raman frequency difference at the first pulse of the interferometer is shifted by the same amount as the selection frequency in order to keep the center velocity class well resonant with the interferometer. Measurements of the gravity shift, in units of μGal, as a function of the offset in the selection frequency are displayed on Fig. 4 as full symbols. For this series of measurements, the Rabi frequency was $\Omega = 2\pi \times 12.5$ kHz.

For a velocity-selection-frequency shift corresponding to the second case (analogous to an uncompensated light shift), we do not observe a significant bias on the Δg measurement (full circles in Fig. 4). In the first case though, which corresponds to a Doppler shift, the asymmetry in the velocity distribution results in a well-resolved bias on the g measurement of $-0.12\,(2)$ μGal/kHz of frequency offset. We take this last result as evidence that the interferometer is not perfectly symmetric. Such a difference between these two cases is expected: in the second case, the shift in the value of g changes sign when changing the direction of the Raman wave vector k, so that the average of the effect over the two k directions is null, whereas it does not change sign in the first case.

We then repeated the same measurements but keeping the Raman frequency at the first pulse fixed, instead of shifting it by the same amount as the selection frequency. The results are displayed as open symbols in Fig. 4. We find as before no effect in the second case (open circles), whereas the effect is much larger in the first case, of $1.44\,(4)$ μGal/kHz (open squares). Indeed, in the first case, the Raman frequency for the interferometer is tuned on the side of the selected velocity distribution, leading to largely unbalanced contributions from opposite-Doppler-shifted velocity classes. The effect is then comparable to the result obtained in Ref. [13], where the Raman frequency of the interferometer was changed without changing the frequency of the selection.

These measurements illustrate the necessity of adjusting the selection frequency onto the center of the initial velocity

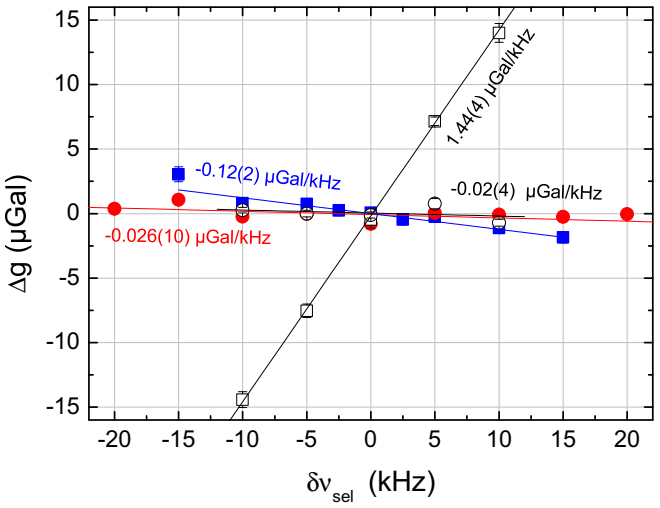

FIG. 4. Effect of an offset $\delta\nu_{\rm sel}$ around the velocity frequency selection $\nu_{\rm sel}$. Squares (circles) show differential measurements corresponding to a Doppler (light shift) effect. The interferometer Raman frequency is (not) shifted according to the $\delta\nu_{\rm sel}$ for the solid colored (not solid colored) symbols.

distribution, and the Raman frequency onto the center of the selected velocity distribution. Any mistake in the adjustment of the corresponding Doppler shifts will lead to an error in the gravity measurement.

V. COMPARISON WITH SIMULATION

In order to compare the previous measurements with their expectations, we developed a numerical model of the experiment by performing a Monte Carlo simulation. The atoms are drawn randomly in a Gaussian position distribution of $\sigma = 0.5$ mm and in a Lorentzian b velocity distribution, with parameters $v_c = 16.5$ mm and $b = 2.4$. These parameters are extracted from a fit of the measured velocity distribution with a Lorentzian b function, which adjusts better the velocity distribution than a Gaussian distribution. The Raman beam is modeled with a Gaussian beam with a 12 mm waist. The simulation includes the effect of the Raman velocity selection. It calculates the evolution of the atomic state in the interferometer, taking into account the trajectory of the atoms in the laser beams (and thus the coupling inhomogeneities), the Raman frequency shifts (such as due to Raman detuning and one-photon light shifts [15]). The response of the detection, which we discuss in more detail in Sec. VII, is also included. It weights differently the contribution of the different velocity classes of the atomic cloud in a manner that depends on the timing parameters. Other systematics, such as two-photon light shifts [22] and Coriolis acceleration, are not expected to influence the effect under study here, which is confirmed by the simulation, that can also take these systematics into account. The number of draws is adjusted for the statistical error to be of order of 0.1 μGal or better. This corresponds typically to 10^6 to 10^7 draws depending on the interferometer parameters.

For the parameters of the results presented above, the simulation predicts in the first case sensitivities of $-0.106\,(3)$ μGal/kHz and $1.36\,(1)$ μGal/kHz, depending on whether the Raman detuning is adjusted or not, and confirms the absence of bias in the second case. These predictions are in fair agreement with the measurements.

VI. INFLUENCE OF INITIAL CLOUD VELOCITY

The velocity distribution just before the selection pulse and, more specifically, its mean value depend on parameters such as the power imbalance of the molasses beams or their polarization state. Fluctuations of the release time from the molasses will also affect the mean velocity just before the selection pulse, as any change in the time interval between release and selection time modifies the velocity change induced by gravity acceleration during that interval.

In this section, we deliberately modify the initial velocity by changing the time of the release from the molasses, keeping all Raman frequencies and timing parameters constant, in order to investigate the influence of variations of this release time onto the gravity measurement. In our experiment, release from the molasses is performed by switching off the laser light with a fast mechanical shutter, controlled by a TTL pulse. Varying the delay parameter t_r of this logic pulse changes the time of the release accordingly.

We then perform (four-configuration) differential measurements in order to measure the change in the gravity values as a function of the change in t_r. We find a linear variation of Δg versus δt_r with a sensitivity of $-5.6\,(1)$ μGal/ms for a Rabi frequency of $2\pi \times 25$ kHz. The linear behavior is well reproduced by the simulation, which gives, for the same parameters, a sensitivity of $-4.23\,(3)$ μGal/ms; about 25% smaller. The difference between the measurements and the simulation can be attributed to imperfect modeling of the initial velocity distribution, or larger coupling inhomogeneities in the experiment than in the simulation. The latter could arise from differences in the intensity profile of the Raman beam: deviation from the ideal Gaussian beam profile could, for instance, be due to speckle or fringes.

We then repeat the measurement of this sensitivity for different Rabi frequencies. The results of these measurements are displayed as gray diamonds in Fig. 5. The results of the simulation, which are displayed as open circles on the figure, show a linear behavior, with a slope of $-0.168(3)$ μGal ms^{-1} kHz^{-1}. A linear fit to the measurements gives here again a significantly larger effect, by about 50%, with a slope of $-0.26\,(1)$ μGal ms^{-1} kHz^{-1}.

As the change of the initial velocity induced by the change in the release time is equivalent to a Doppler shift, we can compare these measurements with the measurements of Fig. 4, where the change was applied on the selection frequency. Given the fact that a change δt_r on t_r gives a change in the Doppler shift of $kg\delta t_r$ of about 25 kHz/ms, the previously determined sensitivity of $-0.12\,(2)$ μGal/kHz of Doppler shift corresponds to a sensitivity of $-3.0\,(5)$ μGal/ms of delay. This result and other such measurements taken for close Rabi frequencies are plotted as blue squares in Fig. 5 and show good agreement with the measurement performed by modifying the release parameter t_r, considering their relatively large error bars. These measurements show that the release time needs to be controlled to better than about 100 μs for accurate

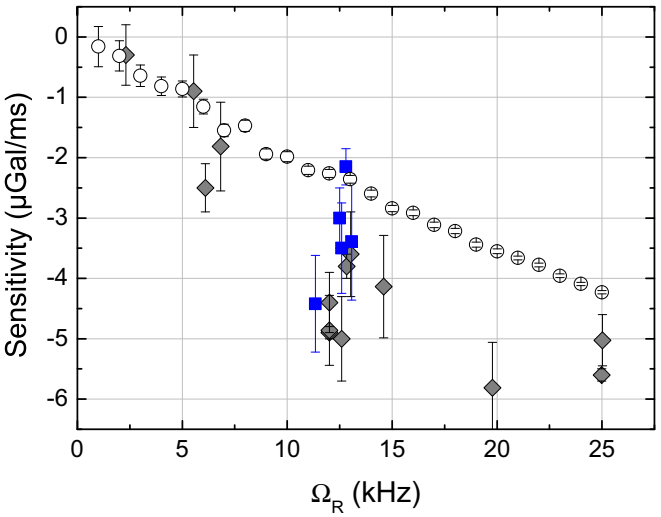

FIG. 5. Sensitivity of the gravity measurement to a change in the release time from the molasses as a function of the Rabi frequency. Gray diamonds show the measurements and open circles show the simulation. Blue squares show the equivalent sensitivities obtained when modifying the selection frequency.

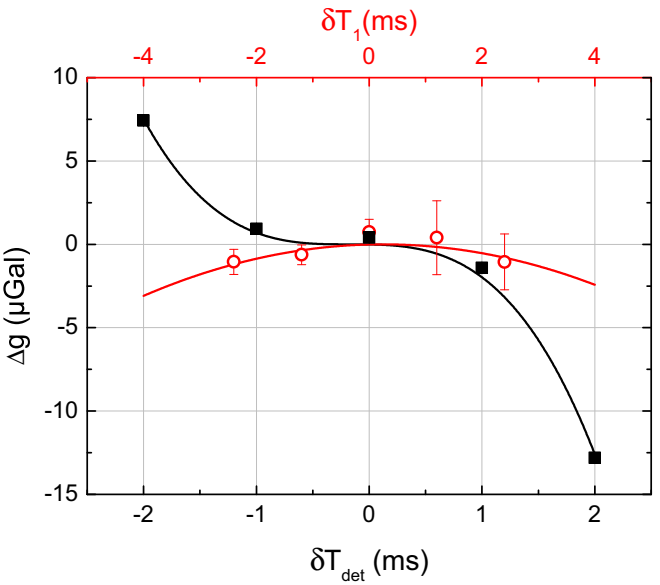

FIG. 6. Influence of the detection timing parameters on the gravity measurements. Black full squares are for scanning only $\delta T_{\rm det}$ [$\delta T_1 = 0$, Fig. 2(b)]. Red open circles are for scanning the position of the two interferometer outputs in a symmetrical way with respect to the center of the detection [$\delta T_1 = -2\delta T_{\rm det}$, Fig. 2(d)]. The black and red lines represent respectively third- and second-order polynomial fits to the results.

measurements at the μGal level. Although such a level of control is easy to reach if using acousto-optic modulators or closed-loop galvos to switch off the light, it is not guaranteed when using open-loop mechanical shutters.

VII. INFLUENCE OF DETECTION PARAMETERS

The weighting of the different velocity classes in the total interferometer phase can also be affected by the detection response. Indeed, after the 200 ms time of flight between the release and the detection, positions in the detection area and atomic velocities are significantly correlated. We then investigate the influence of the detection by adding offsets $\delta T_{\rm det}$ and δT_1 to the two detection timing parameters, which affects the atomic positions in the detection area (see Fig. 2). Because the atomic trajectories are affected by the beam-splitting momentum transfer, optimal detection parameters are different for the two configurations "↑" and "↓," and thus the measurements are performed independently for each wave-vector direction. The results are displayed on Fig. 6 for the ($k_\uparrow$) configuration: $\Delta g = g_\uparrow^{\rm ref} - g_\uparrow^{\rm mod}$ with $g^{\rm ref} = g(T_{\rm det\_ini}, T_{1\_ini})$ and $g^{\rm mod} = g(T_{\rm det}, T_1)$. $T_{\rm det\_ini}$ and T_{1_ini} are the initial parameters, which were estimated thanks to the measurement of the variation of the amplitude of the fluorescence signals versus the detection parameters.

In a first series of measurement, we scan the parameter $T_{\rm det}$ keeping T_1 fixed and we observe an odd dependence (see black squares in Fig. 6). We measure a relatively large bias of order of 10 μGal for large displacements (a 2 ms offset corresponds to a position shift of 4 mm in the detection). Second, we scan the separation between the two clouds in the detection keeping their average position fixed. This corresponds to changing simultaneously T_1 and $T_{\rm det}$ by respectively δT_1 and $\delta T_{\rm det} = -\delta T_1/2$. We observe less pronounced variations with an even behavior. These two series of measurements are difficult to interpret because they correspond to exploring a 2D parameter space along two peculiar lines.

We then compare these measurements with the results of our numerical simulation, varying the detection parameters. Figure 7(a) represents the results of the simulation. It displays the variation of the gravity value with respect to T_1, for various "center time" parameters $T_{\rm c}$ ($T_{\rm c} = T_{\rm det} + T_1/2$) ranging from $T_{\rm c\_opt} + 1$ ms to $T_{\rm c\_opt} - 1$ ms. We observe almost no dependence when $T_{\rm c}$ is well adjusted, and a roughly even dependence if not, similar to our measurement (red curve in Fig. 6). We thus extract two important features from these simulations: (i) the larger the offset with respect to the optimal value of $T_{\rm c}$, the higher the curvature, and (ii) the center of each curve corresponds to the optimum T_1.

In a second step, we performed a series of measurements varying the timing parameters in the same range as in the simulation around their initial values. The results are displayed in Fig. 7(b). We fit the curves with second-order polynomials, from which we extract vertices and curvatures. Figure 8 displays as open squares these curvatures as a function of $\delta T_{\rm c} = T_{\rm c} - T_{\rm c\_ini}$. For comparison, curvatures extracted from simulated data, expressed as a function of $\delta T_{\rm c} = T_{\rm c} - T_{\rm c\_opt}$, are also displayed as full squares. The results of the simulation show a linear behavior, with a slope of 0.537 (3) μGal ms^{-2} ms^{-1} change in $T_{\rm c}$. A linear fit to the data gives a larger slope of 0.81 (7) μGal ms^{-2} ms^{-1} change in $T_{\rm c}$. Remarkably, the linear fit to the measured data crosses zero at $\delta T_{\rm c} \simeq -0.2$ ms, which indicates that the initial value $T_{\rm c\_ini}$ was off by -200 μs with respect to its optimal value.

This illustrates how, by extrapolating the curvature to zero, we can determine $T_{\rm c\_opt}$. In a complementary way, by averaging

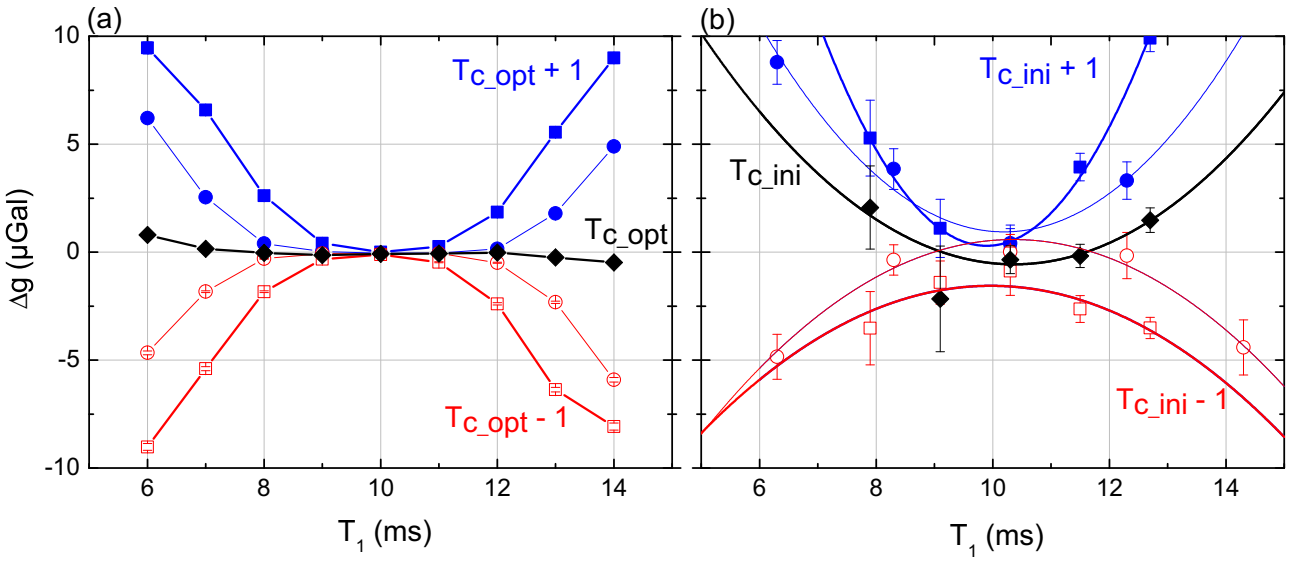

FIG. 7. Influence of the detection parameters. (a) Simulation results for $T_c = T_{c\_opt}$, $T_{c\_opt} \pm 0.5$ ms, $T_{c\_opt} \pm 1$ ms. (b) Measurement results for $T_c = T_{c\_ini}$, $T_{c\_ini} \pm 0.5$ ms, $T_{c\_ini} \pm 1$ ms. Results are fit with second-order polynomials.

the coordinate of vertices, we obtain T_{1_opt}. We thus perform this procedure independently for each direction of the wave vector, because the optimal timing parameters depend on its direction. We find $T_1^{\uparrow} = 9.4\,(3)$ ms, $T_1^{\downarrow} = 9.90\,(5)$ ms, $T_c^{\uparrow} = 298.59\,(6)$ ms and $T_c^{\downarrow} = 299.73\,(5)$ ms. This leads to $T_{det}^{\uparrow} = 293.4\,(2)$ ms and $T_{det}^{\downarrow} = 294.4\,(2)$ ms, close to the expected values, calculated to be $T_{det\_ini}^{\uparrow} = 293.6$ ms and $T_{det\_ini}^{\downarrow} = 294.8$ ms.

We estimate from the results of the simulation that, even for relatively large variations of about ± 1 ms in the parameters T_1 or/and T_{det}, the bias on the g measurement remains smaller than 1 μGal. In particular, the above-mentioned uncertainties in the determination of the optimal parameters lead to a maximum error on the gravity measurements of 0.2 μGal. Finally, we estimated, considering the weak influence of the timing parameters, that the weighting by the detection had no significant impact on the previous measurements of Secs. IV and VI.

VIII. FORCING THE ASYMMETRY

In this section, we introduce controlled asymmetries in the interferometer by deliberately changing the coupling at the last $\pi/2$ pulse, around the typical value of $2\pi \times 12.5$ kHz. We repeat measurements of the sensitivity to the frequency selection by using the protocol described in Sec. IV for different Rabi frequencies of the third pulse: $\Omega_3 = \Omega_{3\_ini} + \delta\Omega_3$. The results, displayed as black dots in Fig. 9, show a monotonic increase of the sensitivity as a function of $\delta\Omega_3$. The results of the numerical simulation are also displayed for comparison (red dots). They show the same behavior as the measurements with an offset of about 0.1 μGal/kHz. Remarkably, the sensitivity to the selection frequency is null

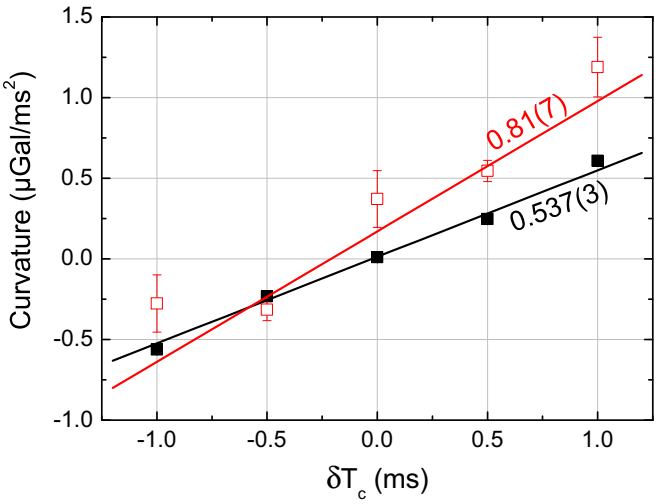

FIG. 8. Measured (open squares) and simulated (full squares) curvatures with respect to the variation of T_c.

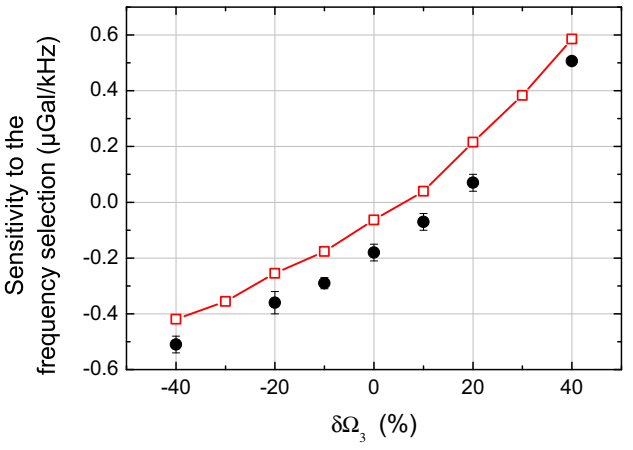

FIG. 9. Sensitivity to the frequency of the velocity selection as a function of the amplitude change of the third Raman pulse. Black full circles represent the measurements and red open squares represent the simulation.

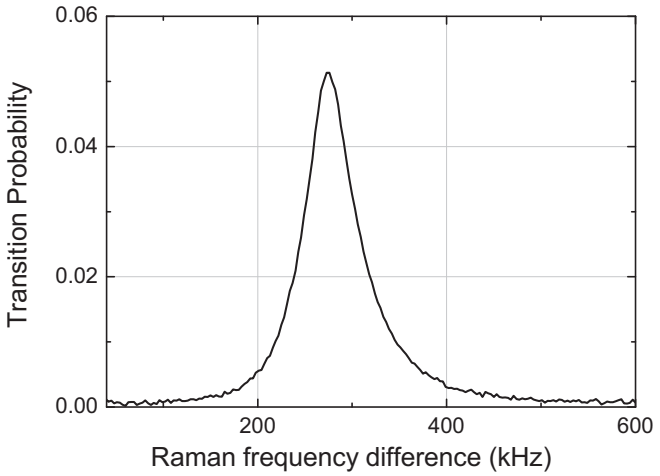

FIG. 10. Raman spectrum of the initial velocity distribution, measured about 12 ms after the release of the atoms from the molasses.

for a change of about 14%. This corresponds to compensating for the asymmetry due to the coupling inhomogeneity by an increase in the coupling. Although this compensation is not independent of the interferometer parameters (for instance, it depends on the initial velocity distribution), it could be of interest for improving the long-term stability of the gravity measurement.

IX. INITIAL VELOCITY DISTRIBUTION

Finally, we characterized the initial velocity distribution because, from the study performed above, we expect that any asymmetry in this distribution will lead to a bias in the g measurement. We thus performed measurements of the velocity distribution with Raman spectroscopy, before selection, by using a long Raman pulse of the order of 100 μs, for which the convolution with the width of the Raman pulse is negligible. The measured Raman spectrum, displayed in Fig. 10, indeed reveals a clear asymmetry in the initial velocity distribution.

The measured distribution was then used to average the phase shift derived in Sec. II for a Rabi frequency of $2\pi \times 25$ kHz and a difference of -14% between the Rabi frequencies at the first and third pulse (which we take here as equivalent to the effect of the inhomogeneities in the Raman coupling due to the transverse spread of the atoms). We found a small effect of -0.60 μGal, that would be the effect in the absence of Raman velocity selection before the interferometer. To determine the effect expected in the case of the velocity selection, we first calculated from the measured distribution the expected velocity distribution after the selection, and averaged the above phase shift with this new distribution. We then found the bias to be significantly smaller: -0.3 μGal.

X. CONCLUSION

We studied the influence of Raman-coupling variations on the symmetry of a Mach-Zehnder interferometer. In the geometry of a free fall gravimeter, where the atoms travel transversally in the Raman beams during the interferometer, coupling inhomogeneities lead to a residual sensitivity of the interferometer phase to the atomic velocity. We show how this effect leads to a bias if the interferometer pulses are not tuned on resonance with the center of the velocity distribution, or if the velocity distribution of the detected atoms is asymmetric. In particular, in our gravimeter, a frequency mismatch of 5 kHz, which is about one order of magnitude smaller than the width of the velocity distribution, leads to a gravity shift of 1 μGal for a Rabi frequency of $2\pi \times 25$ kHz. Our measurements have been compared with a numerical model of the experiment, which reproduces successfully the observed trends, but underestimates the amplitude of the effects by up to 50%. This could indicate that inhomogeneities in the Raman coupling are larger than expected.

Our study highlights the necessity of controlling the initial atomic velocity distribution, which depends on a number of parameters, such as the release time from the molasses and/or the launch velocity, if the interferometer operates in a fountain geometry. Careful adjustments of the frequency of the Raman laser during the selection and interferometer phases, as well as of the timings of our detection, are thus required to reach an accuracy at or below the μGal level.

ACKNOWLEDGMENTS

This research was carried out within the kNOW project, which acknowledges the financial support of the EMRP. The EMRP was jointly funded by the European Metrology Research Programme (EMRP) participating countries within the European Association of National Metrology Institutes (EURAMET) and the European Union. B.C. thanks the Labex First-TF for financial support.

[1] N. Gisin and R. Thew, Nat. Photonics **1**, 165 (2007).
[2] T. D. Ladd, F. Jelezko, R. Laflamme, Y. Nakamura, C. Monroe, and J. L. O'Brien, Nature (London) **464**, 45 (2010).
[3] A. D. Cronin, J. Schmiedmayer, and D. E. Pritchard, Rev. Mod. Phys. **81**, 1051 (2009).
[4] B. Barrett, P.-A. Gominet, E. Cantin, L. Antoni-Micollier, A. Bertoldi, B. Battelier, P. Bouyer, J. Lautier, and A. Landragin, *Proceedings of the International School of Physics Enrico Fermi, Course 188 "Atom Interferometry,"* edited by G. M. Tino and M. A. Kasevich (IOS Press, Amsterdam, The Netherlands, 2014), p. 493.
[5] R. Wynands and S. Weyers, Metrologia **42**, S64 (2005).
[6] J. Kitching, S. Knappe, and E. A. Donley, IEEE Sens. J. **11**, 1749 (2011).
[7] Albert Messiah, *Quantum Mechanics*, Vol. II (North Holland Publishing Company, Amsterdam, 1965).
[8] M. M. T. Loy, Phys. Rev. Lett. **32**, 814 (1974).
[9] E. L. Hahn, Phys. Rev. **80**, 580 (1950).
[10] M. H. Levitt, *Spin Dynamics: Basics of Nuclear Magnetic Resonance* (Wiley, Chichester, 2001).
[11] Ch. J. Bordé, Phys. Lett. A **140**, 10 (1989).
[12] M. Kasevich and S. Chu, Phys. Rev. Lett. **67**, 181 (1991).

[13] A. Peters, K. Y. Chung, and S. Chu, Metrologia **38**, 25 (2001).
[14] N. Ramsey, Phys. Rev. **78**, 695 (1950).
[15] K. Moler, D. S. Weiss, M. Kasevich, and S. Chu, Phys. Rev. A **45**, 342 (1992).
[16] D. S. Weiss, B. C. Young, and S. Chu, Appl. Phys. B: Lasers Opt. **59**, 217 (1994).
[17] P. Cheinet, B. Canuel, F. Pereira Dos Santos, A. Gauguet, F. Yver-Leduc, and A. Landragin, IEEE Trans. Instrum. Meas. **57**, 1141 (2008).
[18] A. Louchet-Chauvet, T. Farah, Q. Bodart, A. Clairon, A. Landragin, S. Merlet, and F. Pereira Dos Santos, New J. Phys. **13**, 065025 (2011).
[19] Ch. J. Bordé, C. R. Acad. Sci. Paris, t.2, Serie **IV**, 509 (2001).
[20] J. Le Gouët, T. E. Mehlstäubler, J. Kim, S. Merlet, A. Clairon, A. Landragin, and F. P. Dos Santos, Appl. Phys. B: Lasers Opt. **92**, 133 (2008).
[21] J. M. McGuirk, G. T. Foster, J. B. Fixler, and M. A. Kasevich, Opt. Lett. **26**, 364 (2001).
[22] A. Gauguet, T. E. Mehlstäubler, T. Lévèque, J. Le Gouët, W. Chaibi, B. Canuel, A. Clairon, F. Pereira Dos Santos, and A. Landragin, Phys. Rev. A **78**, 043615 (2008).
[23] T. Farah, P. Gillot, B. Cheng, A. Landragin, S. Merlet, and F. P. Dos Santos, Phys. Rev. A **90**, 023606 (2014).